Hindawi
International Journal of Intelligent Systems
Volume 2023, Article ID 8863346, 20 pages
https://doi.org/10.1155/2023/8863346

Research Article

Modified Finite Time Sliding Mode Controller for Automatic Voltage Regulation under Fast-Changing Atmospheric Conditions in Grid-Connected Solar Energy Systems

Muhammad Majid Gulzar,[1,2] **Huma Tehreem**,[3] **and Muhammad Khalid**[2,4,5]

[1]*Department of Control & Instrumentation Engineering, King Fahd University of Petroleum & Minerals, Dhahran 31261, Saudi Arabia*
[2]*Interdisciplinary Research Center for Renewable Energy and Power Systems (IRC-REPS), King Fahd University of Petroleum and Minerals, Dhahran 31261, Saudi Arabia*
[3]*Department of Electrical Engineering, University of Central Punjab, Lahore, Pakistan*
[4]*Electrical Engineering Department, King Fahd University of Petroleum & Minerals, Dhahran 31261, Saudi Arabia*
[5]*SDAIA-KFUPM Joint Research Center for Artificial Intelligence, King Fahd University of Petroleum & Minerals, Dhahran 31261, Saudi Arabia*

Correspondence should be addressed to Muhammad Khalid; mkhalid@kfupm.edu.sa

Received 13 January 2023; Revised 23 May 2023; Accepted 5 July 2023; Published 9 August 2023

Academic Editor: Subrata Kumar Sarker

The lack of control in voltage overshoots, transient response, and steady-state error are common issues that frequently occur in a grid-connected photovoltaic (PV) system which can degrade the battery storage and negatively impact other grid components. It may result in damage to equipment and reduce the efficiency of the overall power system. To improve the efficiency of the overall power system, an artificial intelligence (AI) optimization technique is used to determine the optimal sliding mode controller (SMC) gain. The present work proposes the accomplishment of a control strategy for designing a finite-time sliding mode maximum power point controller for a grid-connected photovoltaic (PV) system under fast-changing atmospheric conditions. A particle swarm optimization algorithm (PSO) is used to determine the optimal sliding mode controller (SMC) gains used in perturb and observe (P & O) algorithms. Two modes of operation are available: offline mode for testing different sets of SMC gains leading to optimum values, and online mode for driving the variable step of the P & O MPPT using the SMC optimum gains. The Simscape-power system toolbox (Version 2020A) has been used successfully to study the effectiveness of MPPT. An evaluation of the proposed MPPT compared to the fixed-step P & O is presented. The proposed AI algorithm performs significantly better under fast-changing atmospheric conditions, particularly in transient, steady-state, and dynamic responses. In addition to tuning SMC parameters using PSO, our main contribution is improving the performance of the proposed algorithm to effectively track the maximum power point (MPP) at low oscillation, low ripple, low overshoot, and good rapidity in both slow and fast-changing atmospheric conditions. A three-phase grid-connected PV system with an inverter is described in the present work. The proposed strategy is centered around optimizing the controller of a three-phase grid-connected inverter system in order to improve the power quality.

1. Introduction

A growing dependence on fossil fuels, the need for carbon reduction, and the prospects of developing a new innovative technology sector make photovoltaic (PV) increasingly attractive. Global warming and air pollution are the major issues that have alarming effect on human health [1]. Over the last 20 years, the demand for solar electric power systems has steadily increased, especially since production costs have been reduced and conversion efficiency has increased.

Consequently, global energy investments are shifting towards sustainable energy resources, and renewable energy sources are the more decisive choice for clean energy production [2, 3]. Photovoltaic cells are able to transform the energy from the sun into useable power. When light hits a cell, it generates an electric field across its layers, causing current to flow [4]. An output characteristic that varies with atmospheric conditions, such as temperature and irradiance, that presents two major problems: (a) low efficiency and (b) nonlinearity [5]. The output characteristic of PV-based energy systems is nonlinear because of their weather dependency [6]. Consequently, maximum power point tracking (MPPT) controllers are used to continuously optimize the operating point of PV generators so that the power transferred to the load is as high as possible [7]. This purpose is achieved through a direct and indirect controller. Perturb and observe (P & O) [8], incremental conductance (I & C) [9], and hill-climbing [10] are considered as typical direct techniques. Conversely, maximum power is trailed into two steps. Parameters of the controller are optimized in the first step, and then one of the direct power tracking techniques is implemented. Genetic algorithm [11], artificial neural networks [12], fuzzy logic [13], and particle swarm optimization (PSO) [14] are cited as indirect techniques in the literature. Similarly, other approaches have been used to mitigate the problems associated with solar PV systems (see, e.g., [15–17] and references therein). A direct method with fixed iteration shows satisfactory performance, but the paradoxical challenge arises when choosing a fixed step size. A short step size proffers excellent performance, but it requires significant time to respond. As a result of the long step size, oscillations are being increased around the MPP, and it results in a waste of accessible energy [18, 19]. Modified MPPT algorithms with subduing step size are the best solution to conquer this obstacle. To rebuild the tracking accuracy in modified techniques like the P & O and incremental conductance methods, the step size is modified according to the instinctive characteristics of the PV panel [20].

The role of energy storage devices especially electrochemical battery energy storage in grid-connected solar systems is essential for optimizing their performance and reliability. As renewable energy sources like solar power become increasingly integrated into the grid, energy storage devices play a crucial role in balancing the intermittent nature of solar generation with the fluctuating energy demand. The PV system is classified as a nonlinear system. The use of simple commands and PID correctors has been proven effective for linear systems by researchers. But for nonlinear systems, sometimes they are unable to sufficient.

The integration of unpredictable and uncontrollable solar PV as an energy source in a power grid introduces several challenges into the power grid. Primarily, the transient varying power results in voltage violations at the point of common coupling and additionally contributes towards frequency instability making the entire grid susceptible to catastrophic grid events [21]. In addition, solar PV generates DC power with negligible contribution towards the grid inertia. Therefore, auxiliary power electronic interfaces are pertinent. Furthermore, while solar PV production increases with higher irradiance, its heating also increases with the resulting high-operating, temperatures causing suboptimal production, degradation, and damage [22]. Numerous solutions have been proposed that consists of reactive power support through the PV inverters, inclusion of energy storage devices, utilization of MPPT, and grid support [23]. Nevertheless, the degree of success from any of these solutions is highly dependent on its robustness towards various challenging scenarios of the grid as well as the extreme weather conditions. Utilization of energy storage as a solution might result in accelerated battery degradation due to the high stress current that results from the energy management strategy incorporated [24]. Similarly, effective implementation of PV inverters for voltage regulation can result in an inverter lifetime reduction [25].

As a consequence, we always look for alternative methods to ensure high precision and robustness towards grid components and their applications. The ideology of tracking is pertinent for establishing the framework that can lay for foundation for intelligent computational solutions. Accordingly, we have developed a new MPPT method using a PSO algorithm that optimizes command parameters in finite-time sliding mode. The proposed control scheme is implemented using a synchronous reference frame. This paper consists of designing a definite time controller with a PSO algorithm. Thus, the PSO algorithm is utilized to design the parameters of the controller. The main objective is to obtain optimum values of gains for a finite-time SMC controller in real-time operation, which boosts the power quality performance and makes a PV-based three-phase grid-connected inverter system more stable. The mathematical equation of control design enforces the system to slide on a surface known as a sliding surface. The efficiency of the proposed method is observed by employing a boost converter connected to the PV model. Acquired results validate the efficiency of the proposed controller to trace MPP under an agile change in weather conditions. This work aims to reduce the DC-link voltage fluctuation with a smooth flow of power by stabilizing the frequency of the grid-connected PV inverter in a shorter time.

The novelties of this research study are outlined as follows:

(i) Development of a method with superior performance to conventional algorithm regarding tracking time, preciseness, and competency to track the MPP under various environmental conditions

(ii) Devaluation in the ripple as well as overshoot

(iii) Reduction in response time

(iv) Mitigation of energy losses

The control scheme is designed in MATLAB/Simulink and MATLAB code (m-file) is used for the execution of the PSO algorithm. The simulation results depict excellent performance concerning static and dynamic responses as compared to the classical controllers using fixed-step perturb and observing MPPT.

The paper is organized as follows. A description of a grid-connected PV inverter system is given in Section 2.

The proposed controller is explained in Section 3. The results obtained and the comparative analyses are discussed in Section 4 and Section 5. Conclusions and future directions are presented in Section 6.

2. Description of the Grid-Connected PV Inverter System for the Feedback Control

The grid-connected photovoltaic-based energy system with a three-phase voltage source inverter (VSI) is represented in Figure 1. It consists of a PV-based energy system, MPPT algorithm (P & O), multilevel inverter, and load. The DC-link capacitors at the output terminal of the PV system turn the output voltage from PV to the input voltage for the inverter system. Boost converter step up the input voltages to a higher level, and the MPPT algorithm, as shown in Figure 2, is used to extract maximum power from the energy system.

2.1. Model of the Photovoltaic System. PV cells are considered primitive blocks of a photovoltaic system. These cells are connected in series and parallel to assemble a PV module, and PV modules are used to form an array [26].

The ideal model does not show series and shunt resistances, while the actual model shows those resistances [27]. The equivalent model has been explained in [28]. The PV cell reflects the traits of the diode in the absence of sunlight, and the conversion of energy takes place only in the presence of sunlight [29]. Consequently, the erratic nature of the PV cell makes the system ambiguous. Moreover, the point of stability makes the situation complicated to rely on PV-based energy systems. Thus, a practical model with a single diode is considered, as shown in Figure 3. The PV cell is the elemental unit of the PV system. The output voltage of an individual unit is low. To obtain the desired output current I_{pv} function of the PV array in pragmatic applications, the PV cells are combined in series N_s and parallel connection N_p, as mentioned.

Equation (1) manifests the traits of PV current.

$$I_{pv} = N_p\left[I_{ph} - I_{rs}\left(\exp^{\alpha V_{pv}} - 1\right)\right], \tag{1}$$

where $\alpha = q/N_s \times T \times k \times a$ and V_{pv} are voltage at the output terminal, shows the ideality factor of the diode equation. $q = 1.602 \times 10^{-19}$ C is the charge in an electron, k is the Boltzmann constant $(1.38 \times 10^{-23} J/K)$, N_s is the number of PV cells, and I_{ph} is photocurrent, generated by solar irradiance that can be computed as follows:

$$I_{ph} = 0.01 \times G \times \left[I_{sc} + k_i\left(T^* - T\right)\right], \tag{2}$$

where $G =$ solar insolation; $I_{sc} =$ short circuit current of PV cell; and short circuit current temperature coefficient $k_i = 0.015$ is according to datasheet of PV module. $T^* =$ temperature at Standard test condition (STC) and $T =$ working temperature of the cell. I_{rr} shows reverse saturation current, k shows Boltzmann constant, I_{pv} is the yield current of the PV array, and T is the temperature in the kelvin of PV the cell. Variation in the cell's saturation current (I_{rs}) with temperature has been explained in the following equation:

$$I_{rs} = I_{rr}\left(\frac{T}{T^*}\right)^2 \times \exp\left[\frac{q \times E_g}{k \times a}\left(\frac{1}{T} - \frac{1}{T^*}\right)\right], \tag{3}$$

where E_g represents the band gap energy of semiconductor material of the PV cell.

2.2. DC-DC Boost Converter and MPPT (Perturb and Observe) Technique. The data sheet of the proffered model is shown in Table 1, while the characteristic curves in Figure 2 show the different levels of irradiance level and temperature. Inconsistent variations in solar insolation and temperature have a considerable effect on the voltage and current of the PV array [30].

To track maximum power from the PV array, perturb and observe (P & O) is used together with the DC-DC boost converter. The P & O method is escalated due to its simplicity and ease of implementation [31]. Disturbance in the output voltages of PV panels is based on this algorithm. It is a continual process of disturbance in voltages and then perturbation until concurrence of the operating point occurs at MPP. This algorithm compares the power as well as the voltages of time (K) with a time (K – 1) and anticipates the time to approximate the MPP. A small change in voltage causes agitates in the power of the PV panel. According to the data shown in Table 2, if the alteration is positive, perturbation in voltage is pursued at the same trail. Negative power indicates that MPP is distant and disruption is depreciated to achieve MPP.

The summary of the P & O algorithm is explained in Table 2.

The output voltages V_{pv} can be increased up to 500 v with the variation of duty cycle D of pulse width modulation (PWM) devices in the boost converter. The DC-link assists to reduce the voltage ripple and stabilizes the voltages at the DC-side of the inverter. The boost converter can be explained as follows:

$$V_{dc} = \frac{V_{pv}}{1 - D}. \tag{4}$$

In this research, the prototype model is in MATLAB script editor, while standard test conditions ($G = 1000\, W/m^2$ and $T = 25^{\circ}C$) can generate power 1.04 p.u and $V_{pv} = 0.8$ p.u. Consequently, maximum power point depicts higher efficiency with fewer oscillations.

3. Depiction and Exploration of Proposed Controller

3.1. Modified Finite-Time Sliding Mode Controller. A key feature of this work is to design a mathematical model of the controller for MPPT. Unmodeled dynamics cause external disturbances [33]. Nonlinear controllers are implemented to grasp this ambivalence. The sliding mode controller (SMC) is a kind of nonlinear control. The primitive approach behind this concept is to engage the system trajectory on a sliding surface. Control inputs are mandatory to keep

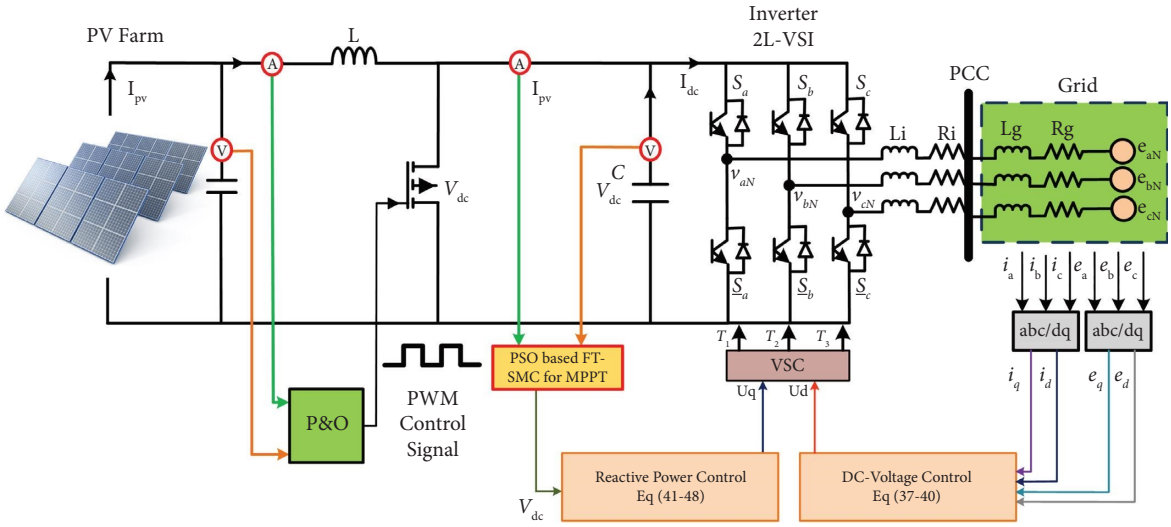

Figure 1: Schematic of feedback control mechanism for the generation of a photovoltaic system.

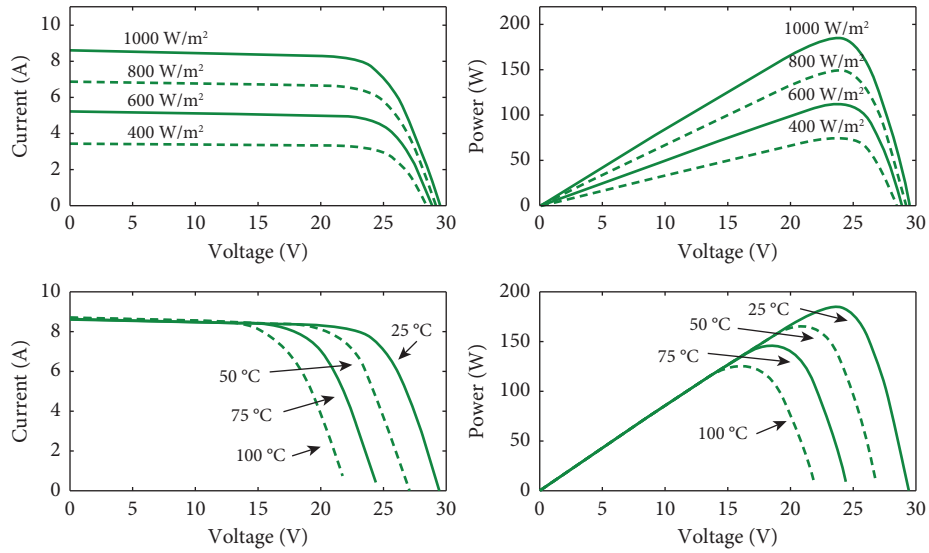

Figure 2: Maximum power point tracking using P & O method.

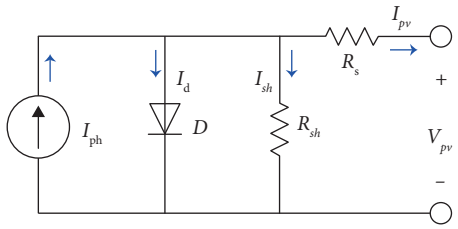

Figure 3: Actual ideal model of the photovoltaic system.

motion trajectories in a predefined surface [34, 35]. In addition, robustness and finite-time convergence make it a more attractive choice [36]. It can be classified into two phases:

(i) Approaching phase

(ii) Sliding phase

Table 1: Data sheet of PV module.

Maximum power	43.68 w
Parallel strings	5
Open circuit voltage	21.90 V
Voltage at maximum power point at STC	0.8 V
Short circuit current	1.00 A
Current at maximum power point	2.55 A
Cell reverse saturation current	$1.2e-7$ A
Temperature coefficient of V_{OC}	−0.36099
Temperature coefficient of I_{SC} (k_i)	0.015
Diode ideality factor	0.32183

The approaching phase is known as the initial phase, where the system trajectory approaches. A nonlinear switching system contingent on time can be illustrated as follows:

Table 2: Scheme of the P & O algorithm [32].

Perturbation	ΔP	Resulting perturbation
+Ve	+Ve	+Ve
+Ve	−Ve	−Ve
−Ve	+Ve	−Ve
−Ve	−Ve	+Ve

$$\begin{aligned} \dot{x} &= f(x.t) + g(x.t), \\ y &= h(x.t). \end{aligned} \tag{5}$$

The state variable is represented by x, while f and g represent smooth vector fields in the same plane, and u represents the discontinuous control exertion. The main purpose is to diminish the error of output variable $e_y = y - y_{ref}$ about zero. $\sigma(x)$ is defined as a certain scaler function of system state tracking error "e" with its higher derivatives like $e^{(1)}, e^{(2)}, \ldots e^{(k)}$:

$$\sigma(x) = f\left(e^{(1)}, e^{(2)}, \ldots e^{(k)}\right). \tag{6}$$

By considering the linear combination of subsequent types as follows:

$$\sigma = e^k + \sum_{i=0}^{k-1} c_i e^i. \tag{7}$$

In a later phase, the system is addressed to the sliding surface in finite time. The sliding phase is not eternal and inconsistency in switching causes the chattering phenomenon. It is the major obstacle in higher-order techniques based on SMC. As a result, degradation in performance occurs. Chattering-free sliding mode characteristics can be achieved by a Lyapunov-based finite-time sliding mode controller (FTSMC). Gains of FTSMC drive the control laws [37]. Consequently, an optimized sliding surface is utilized to propel the variable step size of the classical algorithm of MPPT. SMC manifests precise performance in the existence of ambivalence. Selection of the sliding surface $s(x)$ is the utmost requirement, and state trajectories are intimidated to recline on.

$$s(x) = 0. \tag{8}$$

The chattering phenomenon is a major snag of this control. Transformation of discontinuous control to continuous control is a prerequisite requirement. To converge $V(t)$ to the equilibrium point in a definite time.

$$V(t) + \beta V(t) + \alpha V^{\gamma}(t)) \le 0, \forall t > t_0. \tag{9}$$

While $V(t)$ is a continuous definite function. Convergence of time will take place as follows:

$$t_{ft} \le t_o + \frac{1}{\beta(1+\gamma)} \ln \frac{\beta V^{1-\gamma} t_o + \alpha}{\alpha}, \tag{10}$$

$\alpha > 0, \beta > 0$, and $0 < \gamma < 1$.

3.2. Particle Swarm Optimization. Particle swarm optimization is a scrutinized approach as well as an optimization algorithm. Swarm intelligence is the base of this algorithm. The idea for this algorithm came from the movement of bird and fish flocks. Ease of implementation is the proficiency of this algorithm, and minute rules are simple enough to model the swarm behavior. In research on boid, Reynolds deployed the following three rules.

(i) Step away from the adjacent agent

(ii) Go toward the destination

(iii) Go to the center of the swarm

Simple vectors explain the behavior of the individual agent. Kennedy and Eberhart[38] have explained PSO by assuming birds flocking in two-dimensional space (x, y). While (V_x and V_y) represent the velocities of the axis. The position of the agent is revamped by perceiving the information about the position as well as the velocity of the agent. The advancement of bird flocking is done by a specific function. Individual agent realizes its best value (P_{best}) as well as its x, y position. The aforementioned information is analogous to a particular value of individual agents as well as in the group. It is the accomplishment of the performance of other agents. Individual agent endeavors to adapt their position by utilizing the following information:

(i) The topical current locale (x, y) as well as velocities (V_x, V_y)

(ii) The distance between locales P_{best}

(iii) The distance between locale position g_{best}

The velocity of an individual agent can be reformed by using an adherent set of equations.

$$\begin{aligned} V_i(t+1) &= V_i(t) + c_1 \text{rand}_1\left(p_i - s_i(t)\right) + c_2 \text{rand}_2\left(p_g - S_i(t)\right), \\ s_i(t+1) &= s_i t + V_i(t+1). \end{aligned} \tag{11}$$

While $v_i t$ represents the velocity of the agent i at iteration t; rand_1 and rand_2 show random numbers amongst 0 and 1; locales of agent i at iteration t is shown as $(s_i(t))$; p_i shows p_{best} of an agent i; and p_g shows p_{best} of a group.

Figure 4 reflects algorithmic rules for the development process. The novelty of the proposed work is to utilize algorithmic rules of PSO to accomplish the most advantageous parameters of SMC.

3.3. Implementation of PSO-SMC Variable Step Size P & O MPPT. The sliding surface is defined by a function of discrepancy in voltage and current.

$$x = K_a.dI + K_b.dV + K_c.\text{perturbation}. \tag{12}$$

First order SMC is characterized by

$$\sigma = \frac{dx}{dt} + K_d.x. \tag{13}$$

By using control law, PWM ratio D is driven by SMC.

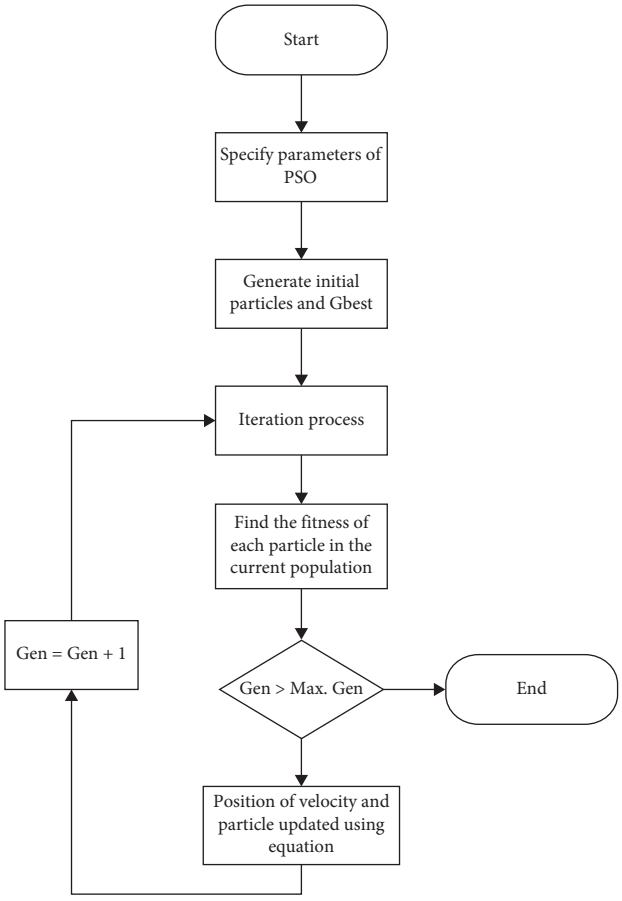

Figure 4: Algorithmic rules for simple PSO.

$$D = K_e.\mathrm{sgn}(\sigma). \tag{14}$$

Gains of SMC (K_a, K_b, K_c, K_d) are optimal by utilizing the PSO algorithm, as shown in Figure 5 and the online and offline modes of the controller are depicted in Figure 6.

The integrated absolute error (IAE) measure is utilized as an objective function (ε) in the following equation :

$$IAE = \int |\varepsilon|\, dt. \tag{15}$$

The manoeuvre of the system consists of two modes.

(i) Offline mode

(ii) Online mode

Various sets of gains of the controller are being tested by using offline mode. Conversely, optimal gains of the controller are used to track the MPP. It can be done by the variation in step size of the P & O MPPT algorithm.

3.4. Model of Voltage Source Control (VSC). The PWM approach is proposed in a three-phase bidirectional DC-AC IGBT-based VSC. Conversion can be done in one or two steps. In one-step conversion, the output power of PV is directly connected to VSC as an input. While in two-stage conversion, the duty cycle of V_{pv}, is calculated. Advancement in the stability edge is the focal point of study by dint of the dynamic model of VSC. Components of current for instantaneous d-q axis are utilized for P-Q control. For this purpose, a phase-locked loop (PLL) is utilized. The control system must be strong enough to grasp the dynamics of PLL. A photovoltaic system is connected with a distribution system via VSC and an assimilate of impedance $R_i + j\omega_e L_i$, ω_e shows angular frequency. While $R_g + j\omega_e L_g$ reflects impedance among points of common coupling if there is an RLC load at PCC.

$$V_{iabc} = L_i p i_{abc} + R_i i_{abc} + V_{sabc.} \tag{16}$$

The dynamic model of VSC in abc frame of reference is expressed in (16). Accordingly, the transformation from abc frame of reference to the d-q reference frame is given in the following equation:

$$p i_{id} = \frac{-R_i}{Li} i_{id} + \omega_e i_{iq} + \frac{(V_{id} - V_{sd})}{L_i.}, \tag{17}$$

$$p i_{iq} = \frac{-R_i}{Li} i_{iq} + \omega_e i_{id} + \frac{(V_{iq} - V_{sq})}{L_i}, \tag{18}$$

$$V_{id} = \frac{mV_{dc}\cos\delta}{\sqrt{2}}, V_{iq} = \frac{mV_{dc}\sin\delta}{\sqrt{2}}. \tag{19}$$

$p = d/dt$ shows the differential operator. While m presents modulation index and δ shows firing angles for VSC.

$$\frac{1}{c}\frac{\partial V_{dc}^2}{dt^2} = P_{pv} - P_{dc}\ and\ P_{dc} = P_t + P_{loss}. \tag{20}$$

Equation (20) shows dynamics of the DC-link capacitor voltages, P_{dc} is the power supply to VSC, and P_t represents active power from the inverter bus. If power losses are abandoned then $P_{dc} = P_t$. PLL-based d-q current model is derived in terms of active and reactive power relation to attain less complex VSC dynamics, and to avoid unnecessary PLL angular frequency calculation at the beginning. At PCC, active and reactive power in the d-q frame of reference is written as

$$P_i = \left(\frac{3}{2}\right)\left(V_{sd}V_{id} + V_{sq}i_{iq}\right), Q_i = \left(\frac{3}{2}\right)\left(V_{sq}i_{id} - V_{sd}i_{iq}\right). \tag{21}$$

In d-q reference, spontaneous current at PCC is written as

$$i_{id} = \frac{2}{3}\left(\frac{P_i V_{sd} + Q_i V_{sq}}{V_s^2}\right), i_{iq} = \frac{2}{3}\left(\frac{P_i V_{sq} + Q_i V_{sd}}{V_s^2}\right), \tag{22}$$

and

$$V_s^2 = V_{sd}^2 + V_{sq}^2. \tag{23}$$

Voltage components V_{sd}, V_{sq} active and reactive powers P_i and Q_i are as follows:

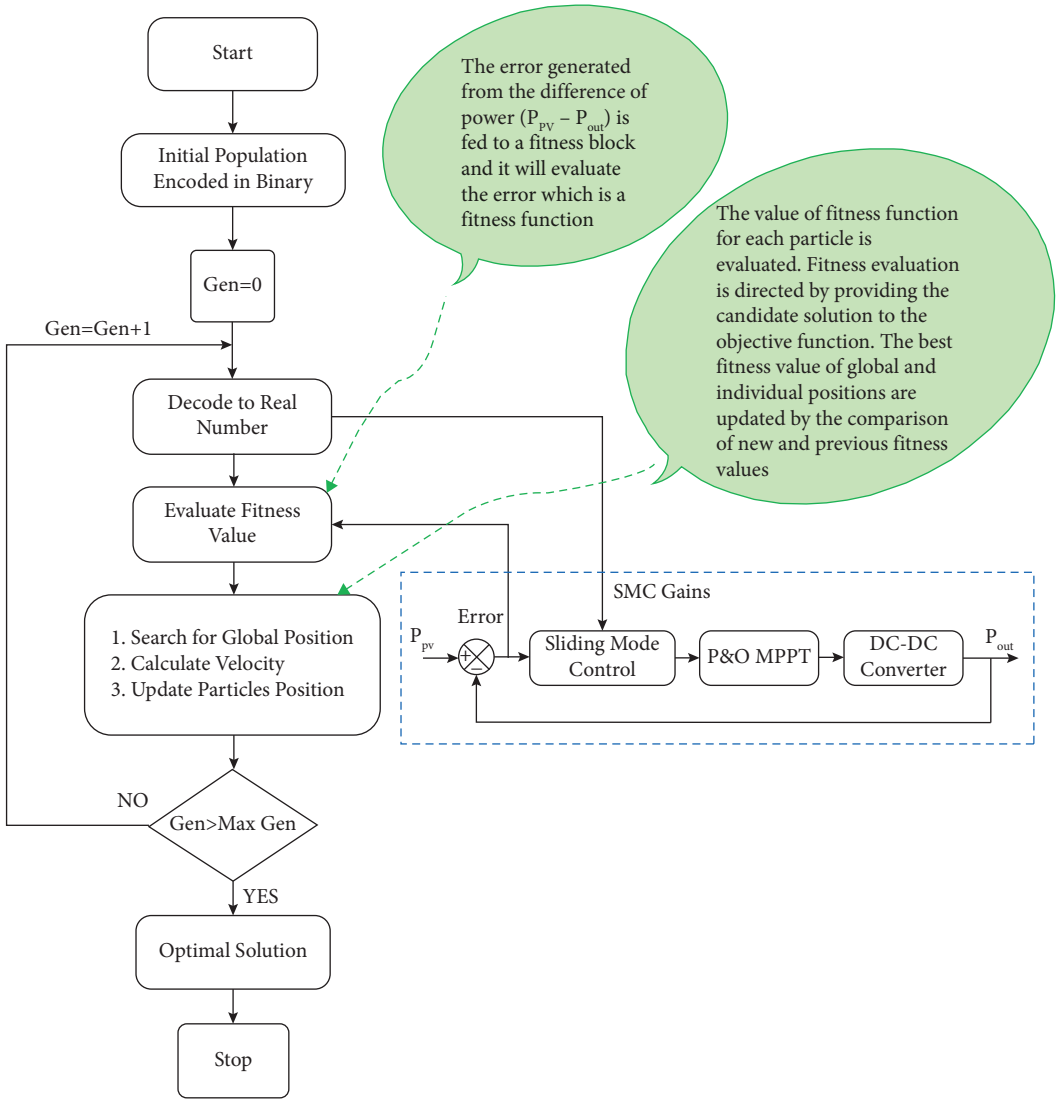

Figure 5: Algorithm for optimization of SMC gains PSO.

$$V_{sd} = \left(\frac{1}{\sqrt{3}}\right)(V_{sb} - V_{sc}), i_{id} = \left(\frac{1}{\sqrt{3}}\right)(i_{ib} - i_{ic}),$$

$$V_{sq} = \left(\frac{2}{3}\right)V_{sa} - \left(\frac{1}{3}\right)(V_{sb} + V_{sc}), i_{iq} = \left(\frac{2}{3}\right)i_{ia} - \left(\frac{1}{3}\right)(i_{ib} + i_{ic}),$$

$$P_i = \frac{3}{2}\left(V_{sd}i_{id} + V_{sq}i_{iq}\right) = \left(V_{sa}i_a + V_{sb}i_{ib} + V_{sc}i_{ic}\right),$$

$$Q_i = \frac{3}{2}\left(V_{sq}i_{id} - V_{sd}i_{iq}\right)$$

$$= \frac{1}{\sqrt{3}}\left[V_{sa}\left(i_{ib} - i_{ic} + V_{sb}\left(i_{ic} - i_{ia}\right) + V_{sc}\left(i_{ia} - i_{ib}\right)\right]. \tag{24}$$

By placing the values of i_{id} and i_{iq} from (22) the following expressions are formulated as follows:

$$\frac{\partial P_i}{\partial t} = \frac{-R_i P_i}{L_i} - \omega_e Q_i + \frac{3}{2L_i}\left[\left(V_{sd}V_{id} + V_{sq}V_{iq}\right) - \left(V_{sd}^2 + V_{sq}^2\right)\right], \tag{25}$$

$$\frac{\partial Q_i}{\partial t} = \frac{-R_i Q_i}{L_i} + \omega_e P_i + \frac{3}{2L_i}\left[\left(V_{sq}V_{id} - V_{sd}V_{iq}\right)\right], \tag{26}$$

$$\frac{\partial V_{dc}}{\partial t} = \frac{1}{CV_{dc}}\left(P_{pv} - P_{dc}\right). \tag{27}$$

P_{dc} shows the active power of VSC. This can be modified by ignoring power losses:

$$P_{dc} = P_{i.} \tag{28}$$

P_i is the active power of VSC at DC-side. Equation (27) can be rewritten as follows:

$$\frac{\partial V_{dc}}{\partial t} = \frac{1}{CV_{dc}}\left(P_{pv} - P_i\right). \tag{29}$$

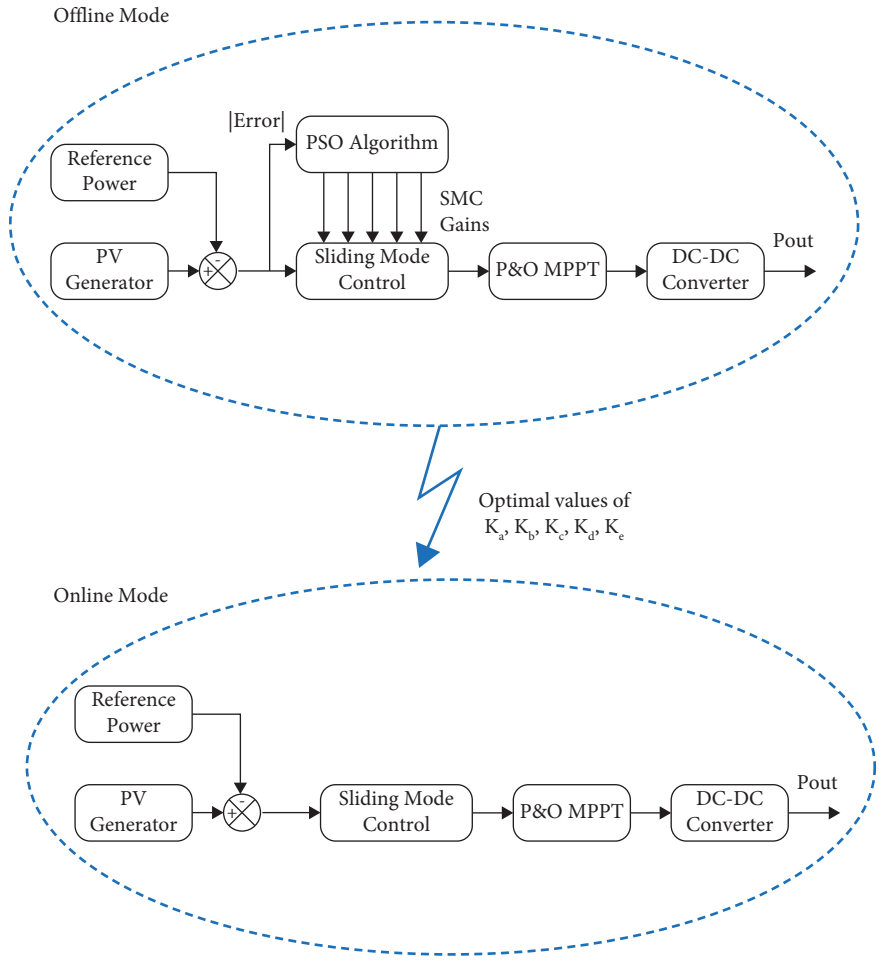

Figure 6: Online and offline method of the proposed controller.

Equations (25), (26), and (29) are used for the dynamic model of VSC-based grid-connected PV system. The operating frequency is achieved during system dynamic operation by a droop control strategy.

$$f - f_o = -R_{droop}\left(P_i - P_{pv}\right). \tag{30}$$

Figure 7 shows the effectiveness of the proposed control over conventional control techniques. In addition, the proposed controller was found more stable and less prone to oscillating characteristics.

3.5. Finite-Time SMC for VSC. The dynamic model to depict nonlinear control for VSC is expressed in (17)–(19). The local frame of reference is chosen to simplify the analysis for VSC. Subsequently, $V_{sd} = V_s$ and $V_{sq} = 0$. Now, power flow to converter becomes simple $P_1 = V_s i_{id}, Q_1 = -V_s i_{iq}$. By implementing the aforementioned transformation, (17)–(19) becomes:

$$\begin{aligned}\frac{\partial P_i}{\partial t} &= \frac{-R_i P_i}{L_e} - \omega_e Q_i + \frac{3}{2L_i}\left[\left(V_s U_d V_{dc} - V_s^2\right)\right],\\ \frac{\partial Q_i}{\partial t} &= \frac{-R_i Q_i}{L_e} + \omega_e P_i + \frac{3}{2L_i}\left[\left(-V_s U_q V_{dc}\right)\right].\end{aligned} \tag{31}$$

While

$$U_d = \frac{m\cos\delta}{\sqrt{2}}, U_q = \frac{m\sin\delta}{\sqrt{2}}. \tag{32}$$

The block diagram of the grid-connected PV system is shown in Figure 8. The overview of the complete model and its feedback control architecture is depicted in Figure 9. The control phenomenon is accomplished by reactive power control and DC voltage control. DC voltage control is explained through (34)–(37). An error signal is calculated in (35) by utilizing the difference between the reference voltage signal and DC voltages. While the equation shows a DC voltage error. The DQ transformation makes the computational process simpler. Using this transformation, three-phase instantaneous voltages and currents are transformed into a DQ frame of reference. The control process becomes more convenient as well. Numerous feedback controllers like PI controller prefer reliable control solution.

4. Controller for Active and Reactive Power

The active and reactive flow of power can be controlled by two output states (Q and V_{dc}). Figure 9 shows that reactive and active power is modulated by AC and DC voltages,

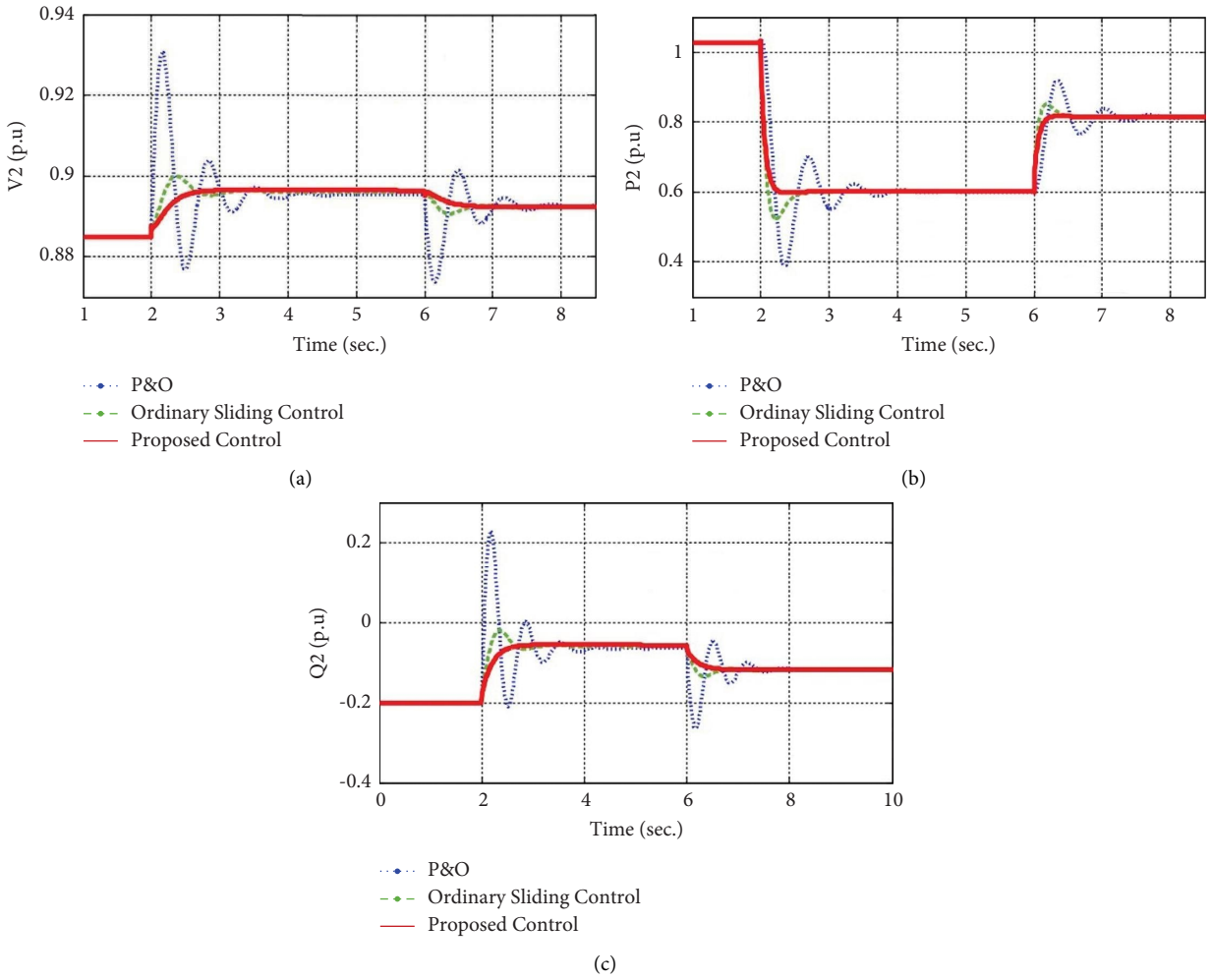

Figure 7: Comparison of the proposed control technique over conventional (at PCC). (a) Voltages at PCC. (b) Active power at PCC. (c) Reactive power at PCC.

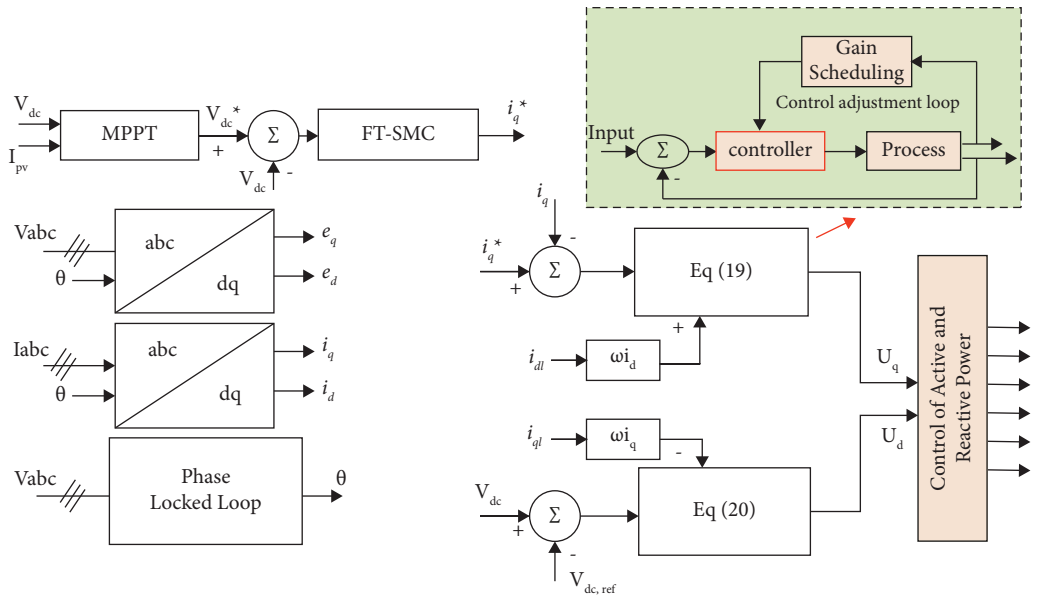

Figure 8: Block diagram for VSC control of the photovoltaic system.

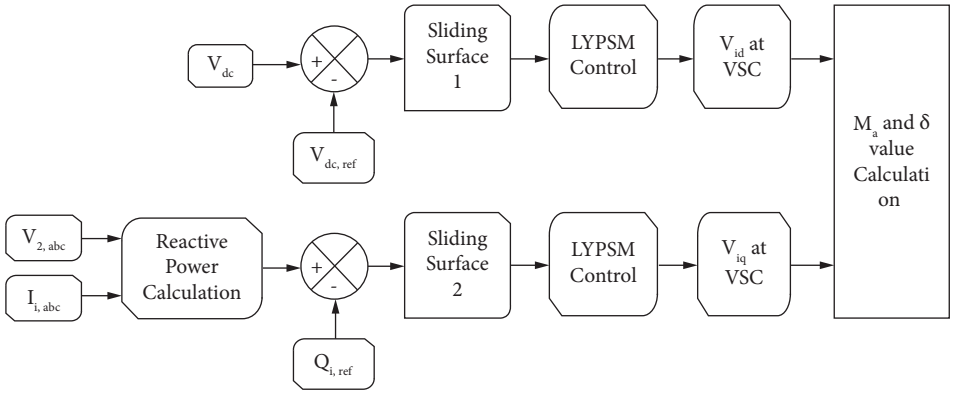

Figure 9: Q-V control for the generation of the photovoltaic system [39].

respectively. The following equations are acquired to accomplish a target

$$u_d = \frac{3V_s^2 + 2R_iP_{iref} + 2\omega_e L_i Q_{iref}}{3V_s V_{dcref}}, \tag{33}$$

$$u_q = \frac{-2R_iQ_{iref} + 2\omega_e L_i P_{iref}}{3V_s V_{dcref}}. \tag{34}$$

Control of DC-link voltage is done by MPPT. Control of reactive power is considered an alternate control variable. Q-V control helps for the accomplishment of control reactive power. The sliding surface is designed in a later stage. Various ways of the establishment regarding DC-link have been discussed in the literature [40]. Multilevel DC-link voltage control develops to extract maximum power from each source of PV.

4.1. Voltage Control of DC-Link. The sliding surface is accomplished after Q-V control. It is established on Q and V_{dc} error following Lyapunov direct stability theorem ($y_1 = V_{dc}, y_2 = Q$) show output states. The error on the PV side is expressed as follows:

$$e_{DC} = V_{dc} - V_{dcref}. \tag{35}$$

$V_{dc} = 1/CV_{dc}(P_{pv} - P_{iref})$ and hence, $P_{iref} = P_{pv}$. The sliding surface for DC-voltage error is given as follows:

$$\dot{e_{\mathrm{DC}}} = \frac{1}{\mathrm{CV_{dc}}}\left(P_{\mathrm{pv}} - P_i\right) - \dot{V_{\mathrm{dc\,ref}}}, \tag{36}$$

$$\sigma_{\mathrm{dc}} = \dot{e_{\mathrm{DC}}} + K_{\mathrm{dc}}\left|e_{\mathrm{DC}}\right|^{q/p}\mathrm{sign}\left(\dot{e_{\mathrm{DC}}}\right), K_{\mathrm{dc}} > 0, q < p, \tag{37}$$

where q and p are positive odd integers. After differentiation and then substitution of the values in (37), we get the following equation:

$$\dot{\sigma_{\mathrm{DC}}} = a_1 - a_2U_d, \tag{38}$$

where

$$a_1 = \left(P_{pv} - P_i\right)K_{dc}\left(\frac{q}{p}\right)\left|e_{DC}\right|^{q/p-1}\mathrm{sign}\left(e_{DC}\right) + \frac{1}{CV_{dc}}\left(\frac{R_iP_i}{L_i} + \omega_eQ_i + \frac{3}{2L_i}V_s^2\right),$$
$$a_2 = \frac{3V_s}{2L_iC}. \tag{39}$$

4.2. Reactive Power Control. Reactive power error

$$e_Q = y_2 - y_{2ref} = Q_i - Q_{iref}. \tag{40}$$

By taking derivative, we obtain

$$\dot{e_Q} = \frac{-R_iQ_i}{L_i} + \omega_eP_i + \frac{U_p}{L_i} - \dot{\mathrm{Q}_{\mathrm{iref}}}. \tag{41}$$

Sliding surface in case of reactive power

$$\sigma_Q = \int_0^t \left(K_{1Q}e_Q + K_{2Q}e_Q^{q/p}\right)\partial t + e_Q, K_{1Q} > 0, K_{2Q} > 0, \tag{42}$$

$$\begin{aligned}\dot{\sigma_Q} &= \left(K_{1Q}e_Q + K_{2Q}e_Q^{q/p}\right) - \frac{R_iQ_i}{L_i} \\ &\quad + \omega_eP_i + \frac{3}{2L_e}\left[-V_sU_qV_dc\right] - \dot{\mathrm{Q}_{\mathrm{iref}}} \\ &= a_3 - a_4U_q,\end{aligned} \tag{43}$$

where

$$a_3 = \left(K_{1Q}e_q + K_{2Q}e_Q^{q/p}\right) - \frac{R_iQ_i}{L_i} + \omega_eP_i - \dot{\mathrm{Q}_{\mathrm{iref}}},$$
$$a_4 = \frac{3}{2L_e}V_sV_{dc}, \tag{44}$$

where K_{1Q} and K_{2Q} control the convergence rate of tracking dynamics. VSC interface is accomplished by positive definite Lyapunov function in (43).

$$V = \frac{1}{2}\sigma_{DC}^2 + \frac{1}{2}\sigma_Q^2, \tag{45}$$

$$\dot{V} = a_1\sigma_{DC} - a_2\sigma_{DC}U_d + a_3\sigma_Q - a_4\sigma_Q U_q, \tag{46}$$

$$U_d = \frac{a_1 + K_1\sigma_{Dc} + K_2|\sigma|^{\lambda}\text{sign}(\sigma_{DC})}{a_2}, \quad K_1 > 0, K_2 > 0, 0 < \lambda < 1, \tag{47}$$

$$U_q = \frac{a_3 + K_3\sigma_Q + K_4|\sigma|^{\lambda}\text{sign}(\sigma_Q)}{a_4}, \quad K_3 > 0, K_4 > 0, 0 < \lambda < 1. \tag{48}$$

If $\dot{V} < 0$ then adherence to the VSC control is guaranteed. Control quantities are described in equations (46)–(48). The Sigma function is implemented to track the dynamics of control. The sign function controls the function of hard switching. Chattering free controller utilizes the tanh function. The Sat function is described as, $sat(\sigma_{DC}) = \text{sign}(\sigma_{DC})$ if $|\sigma_{DC}| \geq 1/\sigma_{DC}$ and alike to σ_{DC}. Implementation of a real-time controller can be considered with the help of the values as explained in equation (48).

$$\tan h(\sigma_{DC}) = \begin{cases} \text{sign}(\sigma_{DC}), & \text{if } \sigma_{DC} \geq 1, \\ \sigma_{DC}|\sigma_{DC}| + 2\sigma_{DC}, & \text{if } \sigma_{DC} < 1. \end{cases} \tag{49}$$

Finite-time control can be accomplished with gains such as K_1, K_2, K_3, and K_4.

$$K_1 = K_{1nom}|\sigma_{DC}|, K_2 = K_{2nom}|\sigma_{DC}|, \quad K_3 = K_{3nom}|\sigma_Q|, K_4 = K_{4nom}|\sigma_Q|. \tag{50}$$

The power-frequency characteristics are as follows:

$$f - f_o = R_{droop}(P_i - P_{pv}), \tag{51}$$

where f_o = nominalfrequency. By utilizing the Lyapunov function in equation (45), robustness and convergence can be accomplished.

4.3. Robustness of LYPSMC. By replacing values of U_d and U_q in (47) as well as (48), we get the following equation:

$$\begin{aligned} \dot{\sigma_{\text{DC}}} &= \frac{1}{CV_{dc}L_i}\left(-K_1\sigma_{Dc} - K_2|\sigma_{Dc}|^{q/p}\text{sign}(\sigma_{Dc})\right) \\ &\quad + K_{dc}\text{sign}(e_{DC})|e_{DC}|^{q/p}\ln(e_{DC})\frac{d}{dt}\left(\frac{q}{p}\right)\sigma_{Dc}, \\ \dot{\sigma_Q} &= -K_3\sigma_Q - K_4|\sigma_Q|^{q/p}\text{sign}(\sigma_Q) \\ &\quad + K_{2Q}(e_Q)^{q/p}\ln(e_Q)\frac{d}{dt}\left(\frac{q}{p}\right). \end{aligned} \tag{52}$$

By applying aforementioned two solutions in (45), we get the following equation:

$$\begin{aligned} \dot{V} &= \frac{1}{CV_{dc}L_i}\left(-K_1\sigma_{Dc}^2 - K_2|\sigma_{Dc}|^{q/p+1}\text{sign}(\sigma_{Dc})\right), \\ &\quad + K_{dc}\text{sign}(e_{DC})|e_{DC}|^{q/p}\ln(e_{DC})\frac{d}{dt}\left(\frac{q}{p}\right)\sigma_{Dc}c, \\ &\quad - K_3\sigma_Q^2 - K_4|\sigma_Q|^{q/p+1}\text{sign}(\sigma_Q) + K_{2Q}(e_Q)^{q/p}\ln(e_Q)\frac{d}{dt}\left(\frac{q}{p}\sigma_Q\right), \end{aligned} \tag{53}$$

where $K_{dc}\text{sign}(e_{DC})|e_{DC}|^{q/p}\ln(e_{DC})d/dt(q/p)\sigma_{Dc}$ and $K_{2Q}(e_Q)^{q/p}\ln(e_Q)d/dt(q/p\sigma_Q)$ are negligible values.

$$\begin{aligned} \dot{V} &= \frac{1}{CV_{dc}L_i}\left(-K_1\sigma_{Dc}^2 - K_2|\sigma_{Dc}|^{q/p+1}\text{sign}(\sigma_{Dc})\right) \\ &\quad - K_3\sigma_Q^2 - K_4|\sigma_Q|^{q/p+1}\text{sign}(\sigma_Q) \leq 0. \end{aligned} \tag{54}$$

The derivative of the Lyapunov function becomes zero far from the limit. It assists in convergent tracking errors at the sliding surface.

4.4. Convergence of LYPSMC. It can be formulated from (37) that whenever tracking error is very adjacent to the origin for convergence $\sigma_{Dc} = 0$ urged convergence in finite time can be achieved.

$$\frac{\dot{e_{\text{DC}}}}{K_{dc}|e_{DC}|^{q/p}\text{sign}(e_{DC})} = -1. \tag{55}$$

By applying convergence limit in integration, we get the following equation:

$$\int_0^{\Delta e_{DC}} \frac{\dot{e_{\text{DC}}}}{K_{dc}|e_{DC}|^{q/p}\text{sign}(e_{DC})}\Delta e_{DC} = \int_0^{\Delta t_o} -1\partial t,$$

$$\Delta t_o = \frac{\dot{e_{\text{DC}}}}{K_{dc}|e_{DC}|^{q/p}\text{sign}(e_{DC})}\Delta e_{DC}. \tag{56}$$

5. Simulation Results

PV-based arrays, as well as IGBT-based VSCs, are utilized in MATLAB simulation. The datasheet of the PV module is conferred in Table 2. PV panel operates at variable temperature and irradiance levels. The PSO algorithm is utilized to tune SMC. It drives the step size which is required by the step size of the P & O algorithm. The duty cycle of the DC-DC converter is driven by this algorithm. At the final stage, the resistive load is powered by a DC-DC converter. Parameters of the PSO algorithm are initialized by simulation. Tables 3 and 4 describe a brief description of grid parameters and PSO parameters, respectively. The gains of SMC are defined in Table 5. Implementation of a PSO-based finite-time sliding mode controller is accomplished with a small population size. In this research, the initial population size is set to be 20 with a maximum of fifty generations ($G = 50$). The objective function fitness value is displayed in Figure 10. A nonlinear load of 1.5 MW,

Table 3: Grid parameters.

Switching frequency	5 kHz
DC-link capacitor	100 μF
Angular frequency (ω)	314.15 rad/sec
Resistance R_i (VSC to PCC)	15 mΩ
Inductance L_i (VSC to PCC)	0.63 mH
R_g (PCC to grid)	10 mΩ
L_g (PCC to grid)	0.5 mH
Line to line voltages	25 kV
System (grid) frequency	60 Hz
Grid side load	30 MW, 2 MVar
Nonlinear load	1.5 MW, 150 KVar

Table 4: Description of PSO parameters.

Description	Parameters
Population size	20
Maximum iteration	50
c_1	2
c_2	2

Table 5: Gains of SMC.

Gains	Values
K_a	3.3823
K_b	−9.1374
K_{C*}	11.17730
K_d	−9.9481
K_c	0.0165

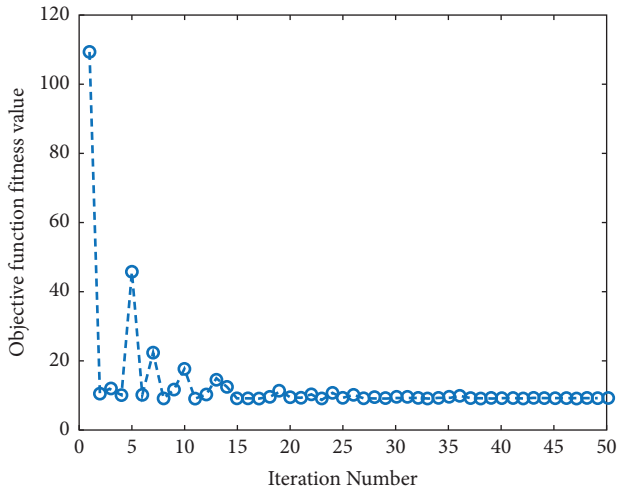

Figure 10: Evolution of objective function fitness values.

150 KVar has been considered, it proves the DC-link stabilization along with controller efficiency.

It is clear that the convergence rate is very quick, especially from iteration 25, where we almost achieved the same fitness. Furthermore, the appraisals consist of two parts as follows:

(i) Standard tests: It comprises three different strategies such as hard, middle, and soft insolation.

(ii) Robustness: It reflects the proposed algorithm for three cases. (a) Variable irradiation level at a constant temperature. (b) Alteration in temperature with fixed traditional level. (c) Alteration in both temperature and irradiance level.

5.1. Standard Tests. Tests comprise three cases as follows:

(i) Hard insulation variation case: Quick variation in immense alteration in irradiance level (400 W/m^2).

(ii) Middle insulation variation case: Quick variation in immense alteration in irradiance level (200 W/m^2).

(iii) Soft variation variation case: Linear irradiation alteration.

After optimization of optimum gains, the controller is used in online mode to drive the variable step size of the P & O MPPT algorithm. These tests consisted of two parts: standard tests and robustness tests. In standard tests, different case studies stimulate hard, middle, and soft insulation. Hard variation is basically abrupt, fast, and large insolation variation (400 W/m^2), middle insulation variation (200 W/m^2), and soft variation linked with linear insulation variation (gradual and soft insulation). Figure 11 displays various points; for instance, A, C, and E display overshoot caused by hard insulation level, as shown in Figure 12, respectively. While B, E, and G show medium insulation which is presented in Figure 13, respectively. Finally, point D depicts soft insolation variation (Figure 14).

5.2. Hard Insolation. In this case, the irradiance level fluctuates (around 400 W/m^2) and causes a negligible change in power (between 0.09 and 0.28 W) for the SMC-based controller whereas the classical controller (which is following the conventional P & O algorithm) shows a significant change in power (from 8.31 to 11.73 W). The proposed controller also reflects a significant improvement in terms of response time under a rapid change in atmospheric conditions (between 40 and 50 ms) compared to (between 133 and 221 ms) for P & O MPPT. Moreover, the proposed algorithm depicts no ripples or oscillations around the MPP, while the conventional controller shows oscillation between 0.029 and 0.27 W. As a result of hard insolation variation, the change in power is minor in the case of the proposed PSO-SMC. The proposed controller shows notable attainment concerning response time during the change in atmospheric conditions. Besides, it also manifests significant accomplishment in steady state with no oscillation around the maximum power point as compared to the classical perturb and observe algorithm between 0.06 and 0.1 W.

5.3. Middle Insolation. Middle insolation is higher or lower than 200 w/m^2. Variation in power manifests from 0.006 to 0.11. Results shown in Figure 15–17 reflect a major improvement in the response time of the proposed controller. This controller also shows no ripple in steady-state error, while the conventional controller shows oscillation around 0.1 W.

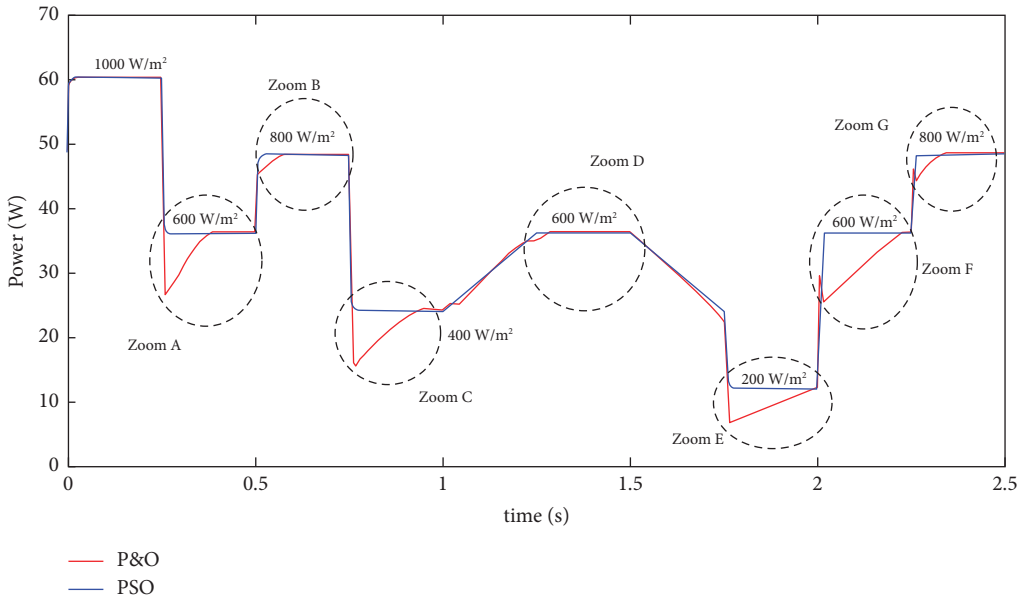

Figure 11: Output power evolution with both MPPT controllers.

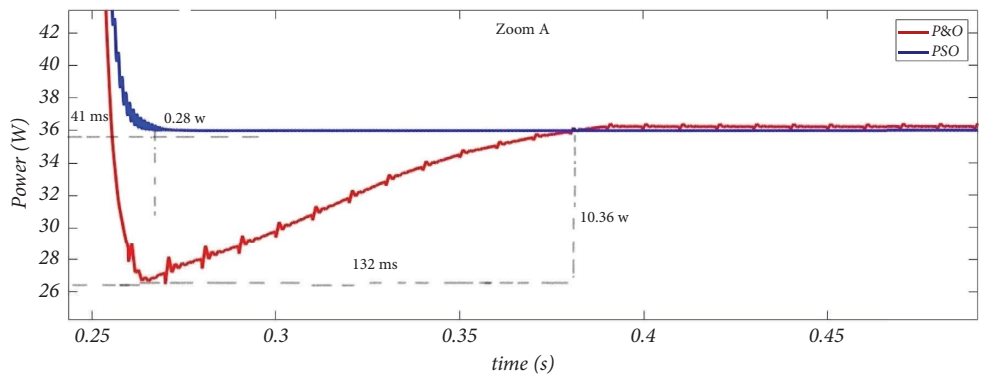

(a)

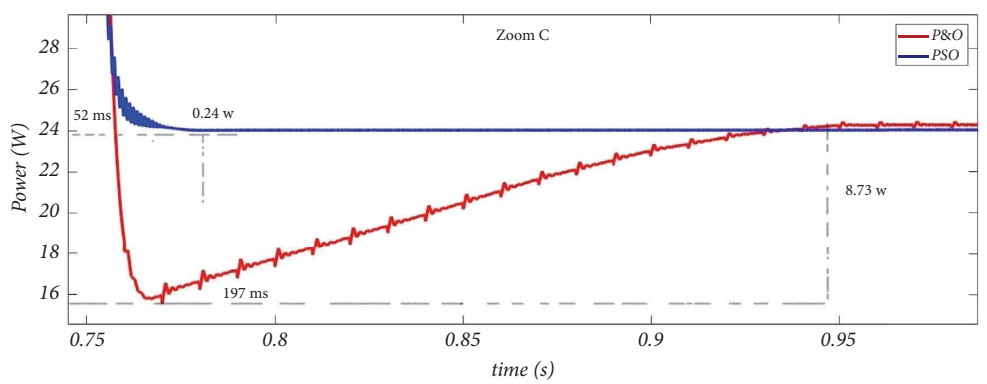

(b)

Figure 12: Continued.

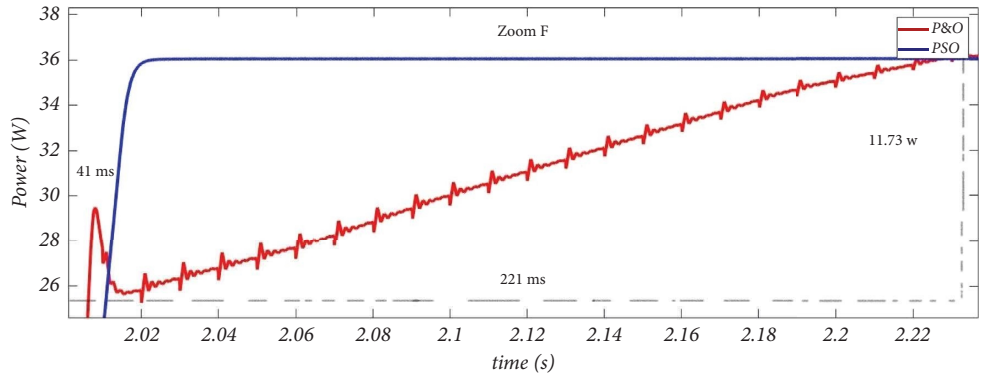

(c)

Figure 12: Hard insolation variation case (comparison of power). (a) Zoom A. (b) Zoom C. (c) Zoom F.

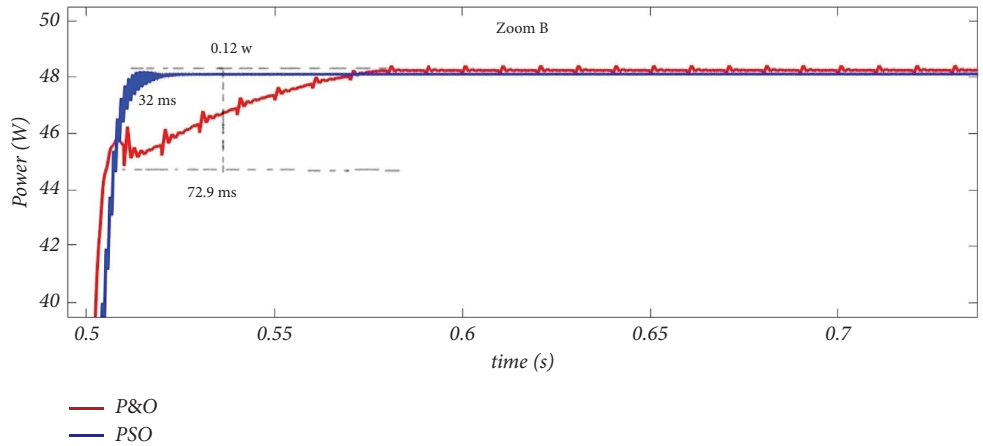

(a)

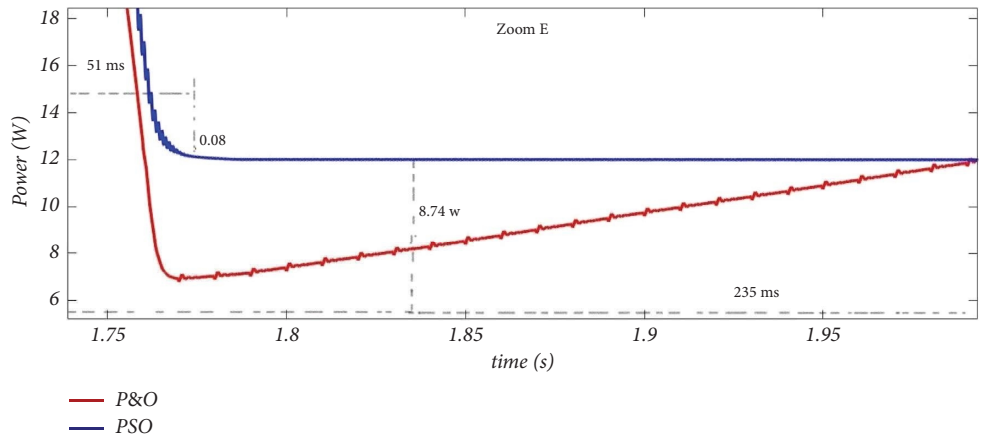

(b)

Figure 13: Continued.

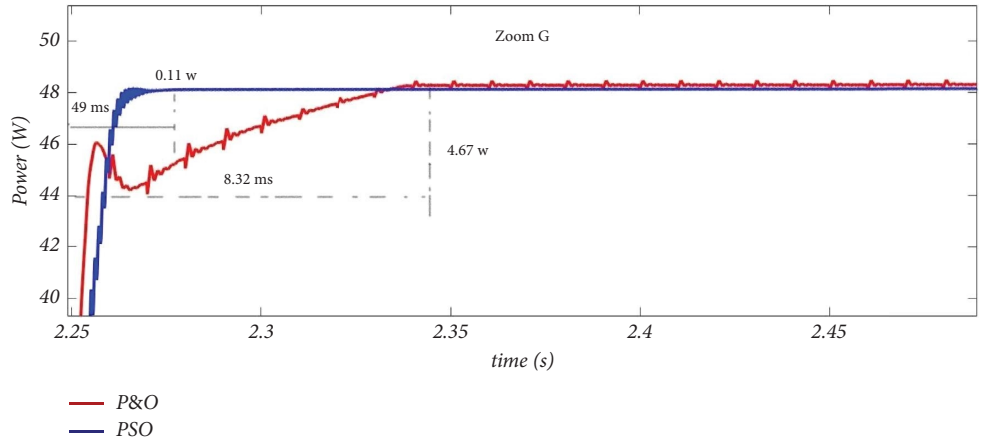

(c)

Figure 13: Middle insolation variation case (comparison of power). (a) Zoom B. (b) Zoom E. (c) Zoom G.

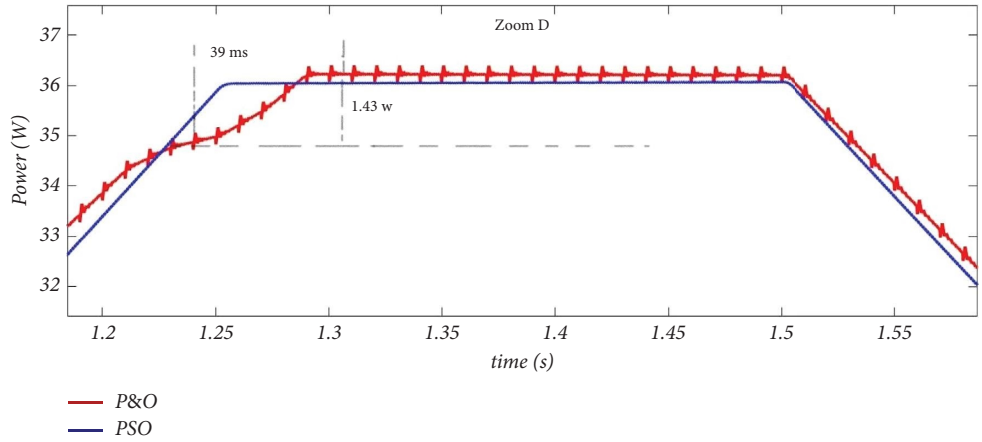

Figure 14: Soft insolation variation case (Zoom D).

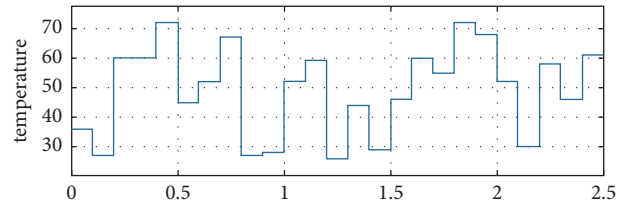

Figure 15: Change in temperature.

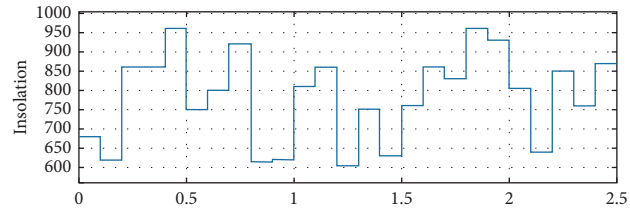

Figure 16: Change in insolation level.

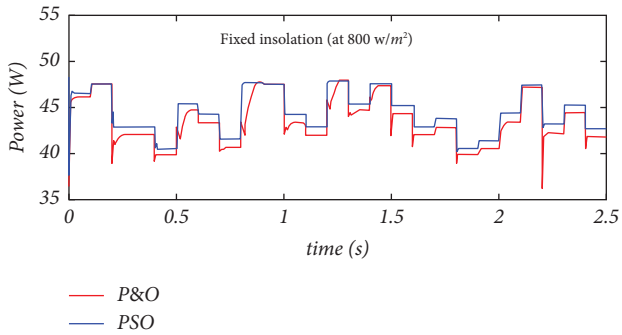

Figure 17: Robustness test at fixed insolation and varying temperature.

Table 6: Standard test results.

Insolation variation	Point	Response time		Overshoot		Ripple	
		P & O	PSOSMC	P & O	PSOSMC	P & O	PSOSMC
Hard	A	133	41	10.36	0.28	0.11	No
	C	197	52	8.73	0.24	0.06	No
	F	221	41	11.73	0.28	0.08	No
Middle	B	72.8	31	3.72	0.11	0.16	No
	E	234	52	5.34	0.09	0.17	No
	G	83.2	49	4.67	0.11	0.16	No
Soft	D	39	0	1.43	0	0.16	No

Table 7: Performance comparison of both algorithms.

Hard insulation variation	P & O/PSOSMC performances at point A: Response time: 133/40 (ms) Overshoot: 10.35/0.28 (W) Ripple: 0.11/0 (W) P & O/PSOSMC performances at point C: Response time: 197/52 (ms) Overshoot: 8.73/0.24 (W) Ripple: 0.06/0 (W) P & O/PSOSMC performance at point F: Response time: 221/41 (ms) Overshoot: 11.73/0.28 (W) Ripple: 0.08/0 (W)
Middle insulation variation	P & O/PSOSMC performance at point B: Response time: 72.8/31 (ms) Overshoot: 3.72/0.11 (W) Ripple: 0.16/0 (W) P & O/PSOSMC performance at point E: Response time: 234/52 (ms) Overshoot: 5.34/0.09 (W) Ripple: 0.17/0 (W) P & O/PSOSMC performance at point G Response time: 83.2/49 (ms) Overshoot: 4.67/0.11 (W) Ripple: 0.16/0 (W)
Soft insulation variation	P & O/PSOSMC performance at point D Response time: 39/0 (ms) Overshoot: 1.43/0 (W) Ripple: 0.16/0 (W)
Summed-up betterments	Response time: <53 (ms) instead of 39–234 (ms) Overshoot: <0.29 (W) instead of 3.72–11.73 (W) Ripples: 0 instead of 0.06–0.17 (W)

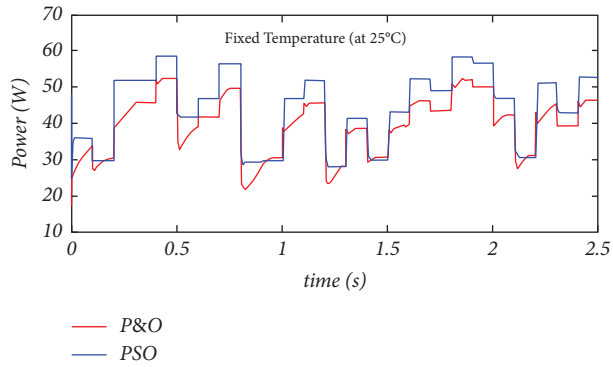

Figure 18: Robustness test at a fixed temperature and varying insolation.

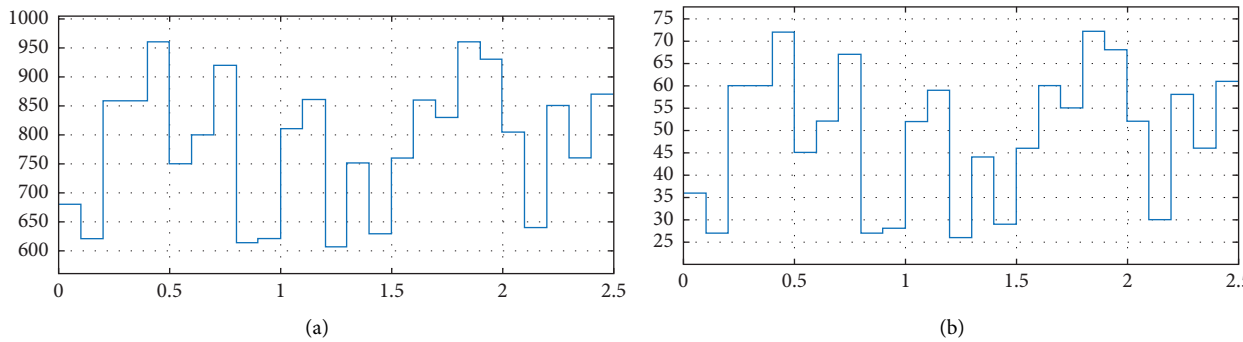

Figure 19: Random insolation and random temperature. (a) Random insolation (W/m^2). (b) Random temperature (°C).

5.4. Soft Insolation. Based on the observations made in Figure 14, the variation in soft insolation shows no ripple in a steady state. It also manifests the properties of low response time as well as low overshoot. The proposed controller reflects an overshoot of 1.42 W with a response time of 38 ms with a ripple around 0.16 W. Therefore, based on the results shown in Figures 11—14 using particular insulation variation schemes (hard, middle, and soft), it can be observed that the presented PSO-SMC variable step size P & O MPPT controller shows a good performance with low overshoot, low response time, and no ripple in the steady state compared with the conventional fixed step size. Table 6 presents the important points by summarising standard tests in tabular form and Table 7 depicts the comparison of both algorithms.

5.5. Robustness Test. The robustness of the controller is tested by variations in temperature (Figure 15) or insolation level (Figure 16) individually. Variation can also be performed by varying the temperature and insolation level in order to validate its efficacy under extreme weather conditions. (a) One thing is clear whenever a variation in irradiance level is observed the temperature is kept constant roundabout 25°. (b) Variation in temperature with a fixed irradiance level of 800 W/m^2. (c) Variation in both temperature as well as irradiance level. Figures 17 and 18 show the results obtained by the proposed controller with the variation of temperature (at fixed irradiance) and irradiance (at fixed temperature), respectively. Figure 19 shows the abrupt change in temperature and insolation at the same time. In addition, a comparison analysis is also performed with conventional P & O MPPT in Figure 20. The proposed controller shows variable step size which reflects notable advancement in an interval of time relative to time concerning variation in weather conditions. The proposed controller shows precise tracking around the MPP point. Test results show the following points:

(i) Benefaction in following rebate in overshoot and ripple

(ii) Advancement in response time

(iii) Competency to accompany maximum power point under a change in atmospheric condition

It results in depletion in power loss.

5.6. Comparative Performance Study of Proposed PSO-Based FTSM Control with Other Existing Control. In this study, a PSO-based sliding mode controller has been presented and examined under rapidly changing atmospheric conditions. A bio-inspired PSO algorithm is used to find the optimum design of the SMC that drives the variable step size of the proposed MPPT algorithm, initially in offline mode. Online testing was then conducted on the optimized SMC.

The combination of particle swarm optimization (PSO) and sliding mode control (SMC) techniques in grid-connected photovoltaic (PV) systems offers significant advantages. PSO, as an artificial intelligence (AI) technique,

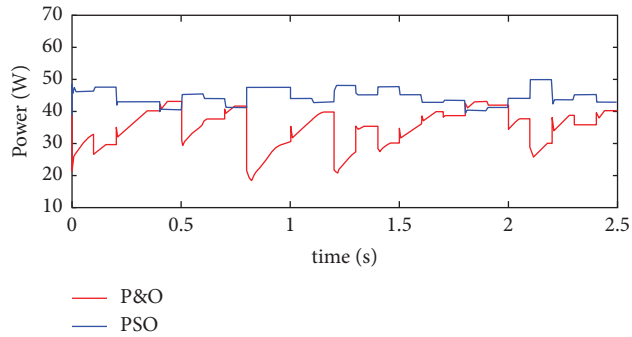

Figure 20: Robustness test at both varying insolation and temperature at a time.

optimizes various system parameters, such as PV array sizing, battery capacity, and control parameters, to maximize energy generation and minimize losses. By iteratively adjusting these parameters based on a fitness function, PSO aids in discovering optimal settings for the PV system. Complementing PSO, SMC provides robust control to manage power flow, battery charging, and grid interaction. SMC ensures a stable grid connection, regulates power flow within desired limits, and effectively manages energy storage devices. The integration of PSO and SMC in grid-connected PV systems leads to enhanced energy efficiency, optimized power flow, improved grid stability, and efficient utilization of energy storage. This synergistic combination of PSO and SMC as AI techniques demonstrates promising potential for enhancing the performance and reliability of renewable energy integration in grid-connected PV systems. The proposed PSO-SMC variable step size P & O MPPT-based algorithm, as well as the conventional fixed step size P & O MPPT algorithm, has both been simulated using the MATLAB/Simulink model, in which different parameters have been implemented. Simulation results demonstrate that the proposed PSO-SMC variable step size P & O MPPT algorithm outperforms the conventional P & O MPPT algorithm in terms of accuracy, rapidity, ripple, and overshoot. There were two types of simulation results: standard tests and robustness tests. A variety of insolation variations were used for the standard tests to obtain results. A comparison was made between the output results of the proposed algorithm and the output results of the P & O algorithm with a fixed step size. A set of parameters is used to extract the data, which is listed in Tables 1–5. The results were presented along with Table 6 summarising the improvements in both transient and steady-state responses confirming that the proposed algorithm outperforms the conventional P & O MPPT regarding all considered performance metrics (response time: < 53 ms instead of 39–234 ms; overshoot: < 0.29 W instead of 3.72-11.73 W; and a ripple: 0 instead of 0.06–0.17 W). In order to demonstrate the robustness and reliability of our proposed algorithm, we tested its ability to track the MPP point under changing atmospheric conditions: insolation of 800 W per square meter at random temperature (Figure 17); random insolation at a fixed temperature ($25^{o}C$) (Figure 18); and variation in both insolation and temperature at random (Figures 19 and 20). As illustrated in Figures 15–19, the proposed algorithm shows comparable results to P & O MPPT. The proposed PSO-SMC variable step size P & O algorithm exhibits a significant improvement in the time interval corresponding to rapidly changing atmospheric conditions, significantly reducing oscillations around the maximum power point. According to the results of the standard and robustness tests, the major contribution of this work was a faster converging speed, less overshoot, no oscillation around the MPP under steady-state conditions, and no divergence from the MPP under fast-varying atmospheric conditions, resulting in an overall reduction in energy losses.

6. Conclusion

Novelty of this work is the combination of an intelligent optimization and a finite-time sliding mode for mitigating the effect of fast varying and extreme weather conditions on renewable-based grids. The aim of this paper is to find the most advantageous layout of the proposed control framework using a variable step size of maximum power point. Various modes of analysis are available for the controller, both online and offline. A MATLAB/Simulink model was used to simulate the proposed controller and the classical controller in order to illustrate their comparative efficacy. A comparative analysis was performed using standard and robustness tests. The standard test consisted of hard, middle, and soft insolation. For the robustness test, random changes in weather conditions were taken into account. In this test, the controllers' performance is evaluated based on overshoot and oscillation around the maximum power point. Observations of steady state and transient responses confirm the outperformance on response time, overshoot, accuracy, and swiftness. Therefore, the resultant facilities reduced the current stress on the battery storage, mitigating its accelerated degradation. The results compiled in the table reflect response time of the proposed controller to around 52 milliseconds rather than 38–234 milliseconds. During abrupt atmospheric changes, the controller shows less overshoot with convergence speed and no divergence around MPP. A reduction in energy losses is also achieved. Hardware-in-loop validation can be planned on an experimental platform to validate PSO-FTSMC.

Data Availability

No underlying data were collected or produced in this study.

Conflicts of Interest

The authors declare that they have no conflicts of interest.

Acknowledgments

The authors would like to acknowledge the support received from Saudi Data and AI Authority (SDAIA) and King Fahd University of Petroleum and Minerals (KFUPM) under SDAIA-KFUPM Joint Research Center for Artificial Intelligence Grant no. JRC-AI-RFP-08, Dhahran 31261, Saudi Arabia.

References

[1] F. Perera and K. Nadeau, "Climate change, fossil-fuel pollution, and children's health," *New England Journal of Medicine*, vol. 386, no. 24, pp. 2303–2314, 2022.

[2] Z. A. Baloch, Q. Tan, H. W. Kamran, M. A. Nawaz, G. Albashar, and J. Hameed, "A multi-perspective assessment approach of renewable energy production: policy perspective analysis," *Environment, Development and Sustainability*, vol. 24, no. 2, pp. 2164–2192, 2022.

[3] M. M. Gulzar, M. Iqbal, S. Shahzad, H. A. Muqeet, M. Shahzad, and M. M. Hussain, "Load frequency control (lfc) strategies in renewable energy-based hybrid power systems: a review," *Energies*, vol. 15, no. 10, p. 3488, 2022.

[4] U. Khan, M. M. Gulzar, D. Sibtain, H. M. Usman, and A. Hayat, "Variable step size fractional incremental conductance for mppt under changing atmospheric conditions," *International Journal of Numerical Modelling: Electronic Networks, Devices and Fields*, vol. 33, no. 6, 2020.

[5] Q. Meng, Y. Chen, Y. Y. Xiao et al., "Effect of temperature on the performance of perovskite solar cells," *Journal of Materials Science: Materials in Electronics*, vol. 32, no. 10, pp. 12784–12792, 2021.

[6] Q. Li, Y. Tian, D. Wu et al., "The nonlinear dynamic buckling behaviour of imperfect solar cells subjected to impact load," *Thin-Walled Structures*, vol. 169, Article ID 108317, 2021.

[7] A. Almutairi, A. G. Abo-Khalil, K. Sayed, N. Albagami, and N. Albagami, "Mppt for a pv grid-connected system to improve efficiency under partial shading conditions," *Sustainability*, vol. 12, no. 24, Article ID 10310, 2020.

[8] Z. M. Ali, N. Vu Quynh, S. Dadfar, and H. Nakamura, "Variable step size perturb and observe MPPT controller by applying θ-modified krill herd algorithm-sliding mode controller under partially shaded conditions θ-modified krill herd algorithm-sliding mode controller under partially shaded conditions," *Journal of Cleaner Production*, vol. 271, Article ID 122243, 2020.

[9] L. Shang, H. Guo, and W. Zhu, "An improved mppt control strategy based on incremental conductance algorithm," *Protection and Control of Modern Power Systems*, vol. 5, no. 1, pp. 14–18, 2020.

[10] A. Ulinuha and A. Zulfikri, "Enhancement of solar photovoltaic using maximum power point tracking based on hill climbing optimization algorithm," in *Proceedings of the Journal of Physics: Conference Series*, vol. 1517, IOP Publishing, Magelang, Indonesia, October 2020.

[11] D. Saadaoui, M. Elyaqouti, K. Assalaou, D. Ben hmamou, and S. Lidaighbi, "Parameters optimization of solar PV cell/module using genetic algorithm based on non-uniform mutation," *Energy Conversion and Management X*, vol. 12, Article ID 100129, 2021.

[12] M. Hanan, X. Ai, M. Y. Javed, M. M. Gulzar, and S. Ahmad, "A two-stage algorithm to harvest maximum power from photovoltaic system," in *Proceedings of the 2018 2nd IEEE Conference on Energy Internet and Energy System Integration(EI2)*, pp. 1–6, IEEE, Beijing, China, October 2018.

[13] F. Blaabjerg, R. Teodorescu, M. Liserre, A. Timbus, and V. Adrian, "Overview of control and grid synchronization for dis-tributed power generation systems," *IEEE Transactions on Industrial Electronics*, vol. 53, no. 5, pp. 1398–1409, 2006.

[14] J. Liang, S. Ge, B. Qu et al., "Classified perturbation mutation based particle swarm optimization algorithm for parameters extraction of photovoltaic models," *Energy Conversion and Management*, vol. 203, Article ID 112138, 2020.

[15] M. A. Syed and M. Khalid, "Moving regression filtering with battery state of charge feedback control for solar PV firming and ramp rate curtailment," *IEEE Access*, vol. 9, pp. 13198–13211, 2021.

[16] M. A. Syed and M. Khalid, "An intelligent model predictive control strategy for stable solar-wind renewable power dispatch coupled with hydrogen electrolyzer and battery energy storage," *International Journal of Energy Research*, vol. 2023, Article ID 4531054, 17 pages, 2023.

[17] M. Hassan, M. Ali, M. Tayyab et al., "Self-balanced quadruple-boost nine-level switched-capacitor inverter for solar PV system," *Arabian Journal for Science and Engineering*, pp. 1–13, 2023.

[18] I. Y. Fawzy, Y. S. Mohamad, E. G. Shehata, and M. Abd El Sattar, "A modified perturb and observe technique for mppt of integrated pv system using dc-dc boost converter," *Journal of Advanced Engineering Trends*, vol. 40, no. 1, pp. 63–77, 2021.

[19] M. Y. Javed, M. M. Gulzar, S. T. H. Rizvi, and A. Arif, "A hybrid technique to harvest maximum power from pv systems under partial shading conditions," in *Proceedings of the 2016 International Conference on Emerging Technologies (ICET)*, pp. 1–5, IEEE, Islamabad, Pakistan, October 2016.

[20] A. K. Gupta, R. K. Pachauri, T. Maity et al., "Effect of various incremental conductance mppt methods on the charging of battery load feed by solar panel," *IEEE Access*, vol. 9, pp. 90977–90988, 2021.

[21] S. S. Alkaabi, H. H. Zeineldin, and V. Khadkikar, "Short-term reactive power planning to minimize cost of energy losses considering PV systems," *IEEE Transactions on Smart Grid*, vol. 10, no. 3, pp. 2923–2935, 2019.

[22] J. Siecker, K. Kusakana, and B. Numbi, "A review of solar photovoltaic systems cooling technologies," *Renewable and Sustainable Energy Reviews*, vol. 79, pp. 192–203, 2017.

[23] N. Al-Rousan, N. A. Mat Isa, M. K. Mat Desa, and H. Al-Najjar, "Integration of logistic regression and multilayer perceptron for intelligent single and dual axis solar tracking systems," *International Journal of Intelligent Systems*, vol. 36, no. 10, pp. 5605–5669, 2021.

[24] D. Azuatalam, K. Paridari, Y. Ma, M. Förstl, A. C. Chapman, and G. Verbič, "Energy management of small-scale PV-battery systems: a systematic review considering practical implementation, computational requirements, quality of input data and battery degradation," *Renewable and Sustainable Energy Reviews*, vol. 112, pp. 555–570, 2019.

[25] O. Gandhi, C. D. Rodrıguez-Gallegos, N. B. Y. Gorla, M. Bieri, T. Reindl, and D. Srinivasan, "Reactive power cost from PV

inverters considering inverter lifetime assessment," *IEEE Transactions on Sustainable Energy*, vol. 10, no. 2, pp. 738–747, 2019.

[26] A. A. Desai and S. Mikkili, "Modelling and analysis of pv configurations (alternate tct-bl, total cross tied, series, series parallel, bridge linked and honey comb) to extract maximum power under partial shading conditions," *CSEE Journal of Power and Energy Systems*, vol. 8, 2020.

[27] A. M. Humada, M. Hojabri, S. Mekhilef, and H. M. Hamada, "Solar cell parameters extraction based on single and double-diode models: a review," *Renewable and Sustainable Energy Reviews*, vol. 56, pp. 494–509, 2016.

[28] A. Laudani, F. Riganti Fulginei, F. De Castro, and A. Salvini, "Irradiance intensity dependence of the lumped parameters of the three-diodes model for organic solar cells," *Solar Energy*, vol. 163, pp. 526–536, 2018.

[29] M. Iqbal and M. M. Gulzar, "Master-slave design for frequency regulation in hybrid power system under complex environment," *IET Renewable Power Generation*, vol. 16, no. 14, pp. 3041–3057, 2022.

[30] D. Sibtain, M. M. Gulzar, K. Shahid, I. Javed, S. Murawwat, and M. M. Hussain, "Stability analysis and design of variable step-size p&o algorithm based on fuzzy robust tracking of mppt for standalone/grid connected power system," *Sustainability*, vol. 14, no. 15, p. 8986, 2022.

[31] S. Salman, X. Ai, and Z. Wu, "Design of a p-&-o algorithm based mppt charge controller for a stand-alone 200w PV system," *Protection and Control of Modern Power Systems*, vol. 3, no. 1, pp. 25–28, 2018.

[32] R. Alik, A. Jusoh, and T. Sutikno, "A review on perturb and observe maximum power point tracking in photovoltaic system," *TELKOMNIKA (Telecommunication Computing Electronics and Control)*, vol. 13, no. 3, pp. 745–751, 2015.

[33] R. M. Nagarale, B. M. Patre, and B. M. Patre, "Exponential function based fuzzy sliding mode control of uncertain nonlinear systems," *International Journal of Dynamics and Control*, vol. 4, no. 1, pp. 67–75, 2016.

[34] J. Wang, Y. Gao, J. Qiu, and C. Ki Ahn, "Sliding mode control for non-linear systems by takagi–sugeno fuzzy model and delta operator approaches," *IET Control Theory & Applications*, vol. 11, no. 8, pp. 1205–1213, 2017.

[35] A. Levant, "Sliding order and sliding accuracy in sliding mode control," *International Journal of Control*, vol. 58, no. 6, pp. 1247–1263, 1993.

[36] A. Levant, "Universal single-input-single-output (siso) sliding-mode controllers with finite-time convergence," *IEEE Transactions on Automatic Control*, vol. 46, no. 9, pp. 1447–1451, 2001.

[37] M. Xie, M. M. Gulzar, H. Tehreem, M. Y. Javed, and S. T. H. Rizvi, "Automatic voltage regulation of grid connected photovoltaic system using Lyapunov based sliding mode controller: a finite-time approach," *International Journal of Control, Automation and Systems*, vol. 18, no. 6, pp. 1550–1560, 2020.

[38] J. Kennedy and R. Eberhart, "Particle swarm optimization," in *Proceedings of ICNN'95-International Conference on Neural Networks*, vol. 4, pp. 1942–1948, IEEE, Perth, WA, Australia, November 1995.

[39] Q. Hu, "Variable structure maneuvering control with time-varying sliding surface and active vibration damping of flexible spacecraft with input saturation," *Acta Astronautica*, vol. 64, no. 11-12, pp. 1085–1108, 2009.

[40] S. K. Dash and P. K. Ray, "Novel pv-tied upqc topology based on a new model reference control scheme and integral plus sliding mode dc-link controller," *International Transactions on Electrical Energy Systems*, vol. 28, no. 7, 2018.